PHILOSOPHICAL TRANSACTIONS OF THE ROYAL SOCIETY A

Phil. Trans. R. Soc. A (2010) **368**, 4455–4479
doi:10.1098/rsta.2010.0205

INTRODUCTION

Traffic jams: dynamics and control

BY GÁBOR OROSZ[1,2,*], R. EDDIE WILSON[3] AND GÁBOR STÉPÁN[4,5]

[1]*Department of Mechanical Engineering, University of California, Santa Barbara, CA 93106, USA*
[2]*Department of Mechanical Engineering, University of Michigan, Ann Arbor, MI 48109, USA*
[3]*Department of Engineering Mathematics, University of Bristol, Bristol BS8 1TR, UK*
[4]*Department of Applied Mechanics, Budapest University of Technology and Economics, Budapest 1521, Hungary*
[5]*Research Group on Dynamics of Vehicles and Machines, Hungarian Academy of Sciences, Budapest 1521, Hungary*

This introductory paper reviews the current state-of-the-art scientific methods used for modelling, analysing and controlling the dynamics of vehicular traffic. Possible mechanisms underlying traffic jam formation and propagation are presented from a dynamical viewpoint. Stable and unstable motions are described that may give the skeleton of traffic dynamics, and the effects of driver behaviour are emphasized in determining the emergent state in a vehicular system. At appropriate points, references are provided to the papers published in the corresponding Theme Issue.

Keywords: vehicular traffic; congestion; stop-and-go waves; Hopf bifurcation; driver reaction time; unstable waves

> I asked Fermi whether he was not impressed by the agreement between our calculated numbers and his measured numbers. He replied, 'How many arbitrary parameters did you use for your calculations?' I thought for a moment about our cut-off procedures and said, 'Four'. He said, 'I remember my friend Johnny von Neumann used to say, with four parameters I can fit an elephant, and with five I can make him wiggle his trunk'.
>
> (Dyson 2004, p. 297)

1. Background and challenges

The introduction of the assembly line in the automotive industry about a century ago allowed the mass production of automobiles, which, in turn, revolutionized land transportation. At the same time, a problem was also generated that has not yet been resolved: traffic congestion. Since then, researchers from many different disciplines (mathematics, physics and engineering) have targeted this problem,

*Author for correspondence (gabor@engineering.ucsb.edu).

One contribution of 10 to a Theme Issue 'Traffic jams: dynamics and control'.

often using sophisticated mathematical tools brought from their own area of expertise. Also, analogies between traffic flow and other flows (fluid flow, gas flow and granular flow) were established. Although such analogies may help scientists to gain understanding of vehicular systems, it is becoming more and more obvious that traffic flows like no other flow in the Newtonian universe.

To date, a vast number of different models have been constructed, but still no first principles have been established to guide the modelling procedure (if such principles exist at all). In many cases, authors claimed that the developed model described traffic better than models prior to that point, and such claims were often justified by fitting the models to empirical data. The quote at the beginning of this paper tries to illustrate, without questioning the importance of any specific model, that the above approach may easily lead to research capturing, but also missing, some essential characteristics. We believe that another way to conduct research in traffic can be by studying general classes of models and classifying their qualitative dynamical features (including 'hidden' unstable motions) when varying model parameters. To set such a dynamical viewpoint in the traffic community requires a unified mathematical language that allows scientists, working in different disciplines from mathematics through physics to engineering, to communicate. As a first step in this quest, we invited a group of world leading experts working on traffic problems in different fields to submit papers for this Theme Issue. Besides presenting novel results, they emphasize the fundamental dynamical features of traffic from their perspective. The papers published in this theme issue represent the state of the art of traffic science, and they are also aimed to be accessible to a broader audience.

In this introductory paper (that also serves as an introduction to the theme issue), we provide readers with a brief overview of traffic data, modelling, dynamics and control. The presentation here is based on the simplest possible setting, i.e. vehicles following each other on a single lane, but we provide references to articles where such a concept has been extended for multi-lane traffic, junctions, traffic signals and urban traffic. Many of these extensions are also specifically targeted by one or more papers published in the theme issue.

2. Traffic data

By the 1930s, vehicular traffic in the USA had already reached the level that required management. The first step towards this was to collect traffic data. Empirical data were collected by using photographic measurements at cross sections, and the data were summarized by the so-called flux–density or fundamental diagram (FD) where the flux (number of vehicles passing the cross section in unit time) was plotted as a function of the traffic density (Greenshields 1935). Moreover, driver parameters, such as reaction time, were already recorded at that time (Greenshields 1936). Since then, FDs have been used to characterize traffic behaviour. The FD in figure 1*a*, which is reproduced from Kerner (2004), represents data collected from the German A5 autobahn near Frankfurt. Clearly, when constructing an FD, one 'projects' the behaviour of a very high-dimensional system to a very low-dimensional diagram. It is not clear, however, whether a state variable is plotted as a function of a parameter or a state space diagram is created; both interpretations are used in the literature.

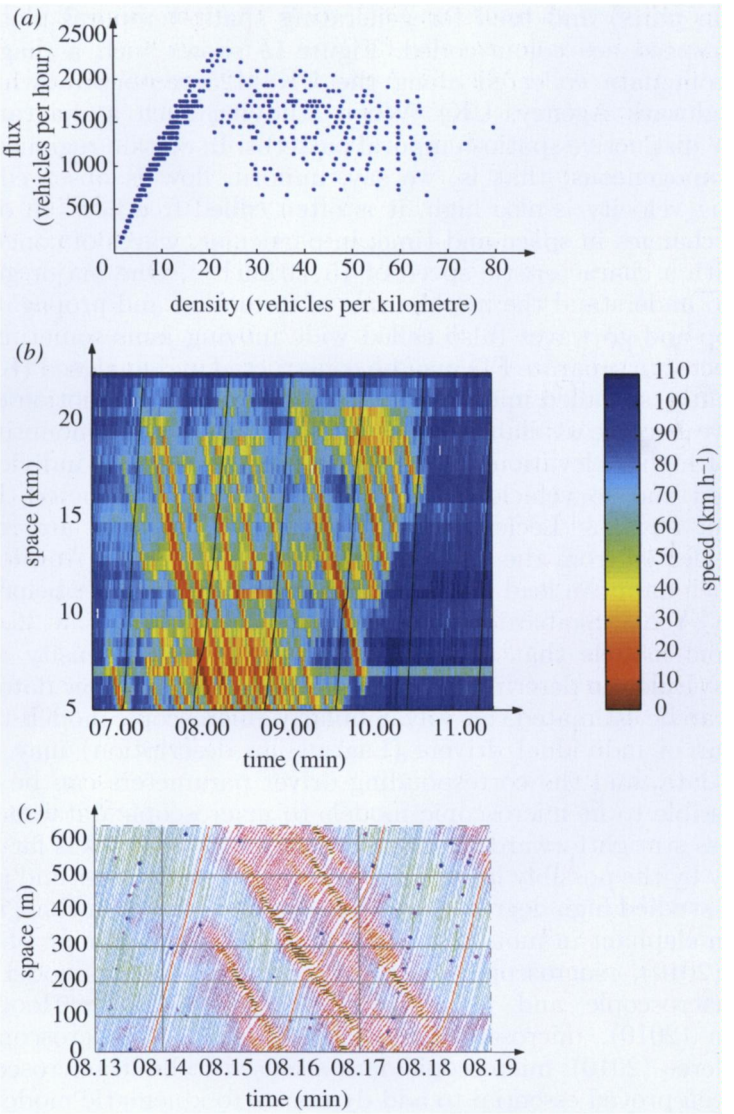

Figure 1. Summarizing traffic data. (*a*) Flux–density diagram constructed from data collected from the German A5 autobahn near Frankfurt—adapted from Kerner (2004). (*b*) Spatio-temporal diagram compiled from data collected from the UK M25 motorway encircling London (Highways Agency, UK). (*c*) Vehicle trajectories reconstructed from camera data collected from the California Highway 101 in Los Angeles—adapted from Laval & Leclercq (2010).

In recent decades, information technology has advanced substantially, and now it allows us to collect 'higher dimensional' traffic data. There are two different approaches used in practice. So-called macroscopic data are collected by installing sensors (usually double induction loop detectors) along the road that measure flux and speed at a certain location, and density may be calculated as the ratio of the two quantities. Usually the data are aggregated in time

(e.g. in 1 min units) and used for generating spatio-temporal plots where the density and speed are colour-coded. Figure 1*b* shows such a diagram that is generated from data collected along the UK M25 motorway, which encircles London (Highways Agency, UK). When studying such a diagram, one may observe some distinctive spatio-temporal patterns. In certain regions, the velocity is almost homogeneous, that is, we say, uniform flow is observed. When the corresponding velocity is also high, it is often called free flow. In other regions the velocity changes in space and time; in particular, waves of congestion travel upstream with a characteristic speed of 15–20 $\mathrm{km\,h^{-1}}$. One major goal in traffic research is to understand the mechanisms of formation and propagation of these so-called stop-and-go waves (also called wide moving jams sometimes). Indeed, for each detector, a separate FD may be constructed and analysed (Kerner 2004).

More recently, so-called microscopic data (describing the motion of individual vehicles) have become available. Such data are collected by mounting a camera on a place of higher elevation or on a helicopter from which individual vehicles can be traced and so vehicle trajectories may be reconstructed. In figure 1*c*, adapted from Laval & Leclercq (2010), vehicle trajectories are reconstructed from data collected from the California Highway 101 in Los Angeles (NGSIM). Analysing such data can lead to better understanding of driver behaviour during car-following (Yeo & Skabardonis 2009).

Macroscopic models that describe traffic in terms of density and velocity distributions (Eulerian description) can be fitted to macroscopic data, and model parameters can be estimated this way. Similarly, microscopic models that describe the behaviour of individual drivers (Lagrangian description) may be fitted to microscopic data, and the corresponding driver parameters can be determined. It is also possible to fit microscopic models to macroscopic data and vice versa, but this is less straightforward. Data-fitting for traffic systems is far from trivial, caused partly by the possibly large number of model parameters and partly by the fact that the studied high degree-of-freedom system changes in time; it is not that easy to fit an elephant in motion (see the quote at the beginning of this paper). In Wagner (2010), macroscopic data are used to estimate model parameters for both macroscopic and microscopic models, while, in Hoogendoorn & Hoogendoorn (2010), microscopic models are fitted to microscopic data. In Laval & Leclercq (2010), microscopic data are used to build microscopic models, and it has been proved essential to add dynamics to kinematic models to be able to reproduce traffic jam formation as observed in data.

3. Traffic modelling

In this section, we give a brief review of the mathematics and physics literature about simplified traffic models; for more discussion, see Helbing (2001) and Nagel *et al.* (2003). We do not attempt to give a complete list of models generated since the 1950s, but rather emphasize the dynamical assumptions behind the classes of models that have shaped traffic research in recent decades. We focus on models that are continuous in time and space, but also mention models where these quantities are discretized. Note that discretizing time and/or space in a multi-scale system may 'wash away' some interesting dynamics and, consequently, may lead to limited or even incorrect conjectures.

Depending on the spatial scales represented, two different classes of models exist. Macroscopic (or continuum) models do not consider individual vehicles but rather describe traffic in terms of continuous density and velocity distributions as functions of space and time. The dynamics, i.e. the time evolution of these distributions, is given by partial differential equations (PDEs). On the other hand, microscopic (or car-following) models describe the behaviour of individual vehicles: discrete entities that move in continuous space. Here, the motion of vehicles is given by ordinary and delay differential equations. Despite six decades of research, the connection between the two classes of models is still not clarified for two main reasons. On one hand, as mentioned above, the viewpoints of the two modelling approaches are different. The Eulerian view of continuum models deals with the changes of density and velocity in time at a fixed location, while, in the Lagrangian view of car-following models, distances and velocities are monitored when 'travelling together with individual vehicles'. Moreover, the relationship between distances and densities is far from trivial in dynamical situations (Berg *et al.* 2000). On the other hand, the psychological actions of drivers make traffic different from any other flow. In this 'fluid', 'particles' (of finite size) interact by violating Newton's Third Axiom since the leader's motion influences the follower's motion but not vice versa—except when collisions occur.

(*a*) *Continuum models*

In continuum models, traffic is described via a density distribution $\rho(x,t)$ and a velocity distribution $v(x,t)$, which are continuous functions of location x and time t. In such models, we have conservation of vehicles, so that in the absence of sources and sinks (on- and off-ramps)

$$\partial_t \rho + \partial_x(\rho v) = 0, \tag{3.1}$$

where ∂ stands for partial differentiation. The quantity $q(x,t) := \rho(x,t)v(x,t)$ describes the instantaneous flux (also called throughput or flow) at location x and time t. Further refinements are possible considering multi-species models, multi-lane configurations and junctions (Daganzo 2002*a*,*b*; Benzoni-Gavage & Colombo 2003).

To complete the model, one needs to define the relationship between density and velocity (or alternatively between density and flux). One possibility is to assign the velocity directly as a function of density (and its spatial derivatives)

$$v = \mathcal{G}(\rho, \partial_x\rho, \partial_{xx}\rho, \ldots). \tag{3.2}$$

Formulae (3.1), (3.2) are often called kinematic or first-order models. In the simplest setting, introduced in Lighthill & Whitham (1955), we have

$$v = \mathcal{V}(\rho), \tag{3.3}$$

where $\mathcal{V}(\rho)$ is a decreasing function, modelling that dense traffic should travel slower than sparse traffic for safety reasons. Equivalently, the flux can be assigned as $q = \rho v = \rho\mathcal{V}(\rho) := \mathcal{Q}(\rho)$. If one initializes this model so that fast traffic is placed behind slow traffic, the solution profile sharpens and a discontinuous shock develops in finite time where the velocity jumps downwards, requiring infinite deceleration.

To represent vehicles' inertia, dynamic or second-order models may be constructed where formula (3.1) is supplemented with an equation for the acceleration (i.e. the total derivative of the velocity)

$$\partial_t v + v\partial_x v = \mathcal{F}(\rho, \partial_x \rho, \partial_{xx}\rho, \ldots, v, \partial_x v, \partial_{xx} v, \ldots). \tag{3.4}$$

As a matter of fact, most models in the literature can be written in the specific form

$$\partial_t v + v\partial_x v = \frac{1}{T}(\mathcal{V}(\rho) - v) + \mathcal{N}(\rho, \partial_x \rho, \partial_{xx}\rho, \partial_x v, \partial_{xx} v). \tag{3.5}$$

The first term on the right-hand side corresponds to relaxation to a density-dependent optimal velocity given by the decreasing function $\mathcal{V}(\rho)$ with a relaxation time T. The limit $T \to 0$ suggests a connection with equation (3.3). Note that this idea also appears in microscopic models as explained further below. The second term is such that $\mathcal{N} = 0$ for constant density and velocity, in which case equation (3.3) still holds. This term may be constructed using fluid dynamical analogies and usually contains a 'pressure term' that is proportional to $-\partial_x \rho/\rho$ and represents anticipation of drivers to events ahead, and a 'diffusion term' that is proportional to v_{xx} and represents the averaged effects of noise (Payne 1979; Kerner & Konhäuser 1994).

Despite the fact that pressure and diffusion are abstractions that are difficult to interpret in traffic, these models are able to reproduce uniform flow as well as stop-and-go waves (without discontinuities). However, they have been criticized for predicting non-physical flow motions (negative flux and negative velocities) under certain conditions (Daganzo 1995). In response to this criticism $\mathcal{N} = \rho\mathcal{P}'(\rho)\partial_x v$ has been proposed by Aw & Rascle (2000), where the function $\mathcal{P}(\rho)$ represents anticipation. Moving $\mathcal{N}$ to the left-hand side and using equation (3.1), model (3.5) can be rewritten as

$$\partial_t(v + \mathcal{P}(\rho)) + v\partial_x(v + \mathcal{P}(\rho)) = \frac{1}{T}(\mathcal{V}(\rho) - v). \tag{3.6}$$

Here $v + \mathcal{P}(\rho)$ represents a Lagrangian quantity and the model is claimed to properly describe the anisotropy of traffic flow: particles respond to stimuli from the front but not from the back. Notice that model (3.1), (3.6) is a hyperbolic PDE with a source term on the right-hand side. Continuum models can also be developed from microscopic models, yielding the form (3.5) where the spatial derivatives appear owing to the discrete-to-continuous transformation (Berg *et al.* 2000). Time delays may also be included in continuum models (Siebel & Mauser 2006) to mimic driver reaction time. As will be shown below, reaction time is an essential element of car-following models, but it is not clear how it should be incorporated in continuum models. Noise may also be added explicitly to any of the above models, but it has rarely been done in the literature.

The advantages of continuum models are that the results can be directly compared with macroscopic data, such as the FD in figure 1*a* and the space–time diagram in figure 2*b* (Kerner 2004), and that it is also relatively easy to provide the boundary conditions for velocity and flux. Their disadvantage is, however, that it is difficult to relate the model parameters to microscopic driver parameters. Moreover, it is not clear what limitations are imposed by the fact that fundamentally discrete systems are being modelled as continua.

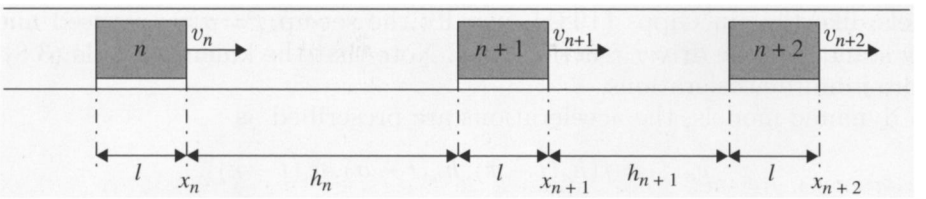

Figure 2. Sequence of cars on a single-lane road showing vehicles' positions, velocities and headways.

Finally, we remark that there are Boltzman-type gas-kinetic models, which are based on collisions of particles and contain noise explicitly (Prigogine & Herman 1971; Helbing 1995), but these cannot be presented in the form of (3.1), (3.2) or (3.1), (3.4).

(*b*) *Car-following models*

In car-following models, discrete entities move in continuous time and continuous space, as shown figure 2, where vehicles of equal length ℓ are plotted in a specific setting. At time t, the position of the front bumper of the nth car is denoted by $x_n(t)$, its velocity is $v_n(t)$ and the bumper-to-bumper distance to the vehicle in front (called the headway) is $h_n(t)$. Differentiating $h_n(t) = x_{n+1}(t) - x_n(t) - \ell$ with respect to time t and using $\dot{x}_n(t) = v_n(t)$, one obtains

$$\dot{h}_n(t) = v_{n+1}(t) - v_n(t). \tag{3.7}$$

To complete the model this equation has to be supplemented with a car-following rule, that is, the velocity or the acceleration has to be given as the function of stimuli that are usually the distance h_n, the velocity difference $\dot{h}_n$ and the vehicle's own velocity v_n. Note that some models also contain the velocity v_{n+1} and/or the acceleration $\dot{v}_{n+1}$ of the leader, which will not be explicitly represented by the notation used below. To further simplify the matter, drivers with identical characteristics are often considered.

When velocities are assigned, the corresponding kinematic models can be written in the form

$$v_n(t) = g(h_n(t-\tau), \dot{h}_n(t-\sigma), v_n(t-\kappa)), \tag{3.8}$$

which are sometimes called collision avoidance models (Kometani & Sasaki 1958). At least one of the delays τ, σ, κ has to be positive to obtain a feasible model, but it is not always obvious what these quantities physically mean. For example, in the model $v_n(t) = v_{n+1}(t-\sigma)$, the delay σ stands for a time gap (a time distance the driver keeps from the leader; Newell 2002), while in the model

$$v_n(t) = V(h_n(t-\tau)) \tag{3.9}$$

the delay τ may represent a reaction time (a dead time required to process information and initiate action) and/or a relaxation time (that corresponds to the driver's reaction inertia; Newell 1961, 2002; Igarashi *et al.* 2001). Here, $V(h)$ is an increasing function that represents that the larger the headways are, the faster the drivers intend to go. To establish a connection between models (3.3) and (3.9), one may define $\mathcal{V}(\rho) := V(1/\rho - \ell)$. In more complicated kinematic

models, like that in Gipps (1981), usually the set-up $\tau = \sigma = \kappa$ is used and the delay stands for the driver reaction time. Note that the kinematic rule (3.8) may require infinite accelerations.

In dynamic models, the accelerations are prescribed as

$$\dot{v}_n(t) = f(h_n(t-\tau), \dot{h}_n(t-\sigma), v_n(t-\kappa)), \tag{3.10}$$

where τ, σ, κ represent driver reaction times to different stimuli. As will be shown below, these are different from the time gap and from the relaxation time. To make the model more tractable, simple relations may be assumed between the different delays. There are three simplifications commonly used in the literature:

— *Zero reaction times*: $\tau = \sigma = \kappa = 0$. This is usually justified by saying that dynamic models (3.10) may reproduce uniform flow as well as stop-and-go waves for zero reaction time by varying some other characteristic times (Bando *et al.* 1995).
— '*Human driver set-up*': $\tau = \sigma > 0, \kappa = 0$. This set-up represents that drivers react to the distance and to the velocity difference with (the same) delay, but they are aware of their own velocity immediately (Gazis *et al.* 1961; Davis 2003; Orosz *et al.* 2009).
— '*Robotic driver set-up*': $\tau = \sigma = \kappa > 0$. This set-up is mainly used in the adaptive/automatic/autonomous cruise control (ACC) literature. The delay is introduced to account for the time needed for sensing, computation and actuation in computer-controlled vehicles (Kesting & Treiber 2008; Orosz *et al.* 2010).

Many other set-ups are also possible; for example, one may account for human memory effects by using distributed delays, as in Sipahi & Niculescu (2010).

Early dynamical car-following models, such as those in Gazis *et al.* (1961), took the form

$$f(h, \dot{h}, v) = \frac{1}{T} \frac{\dot{h}^q v^r}{h^p}, \quad p, q, r \in \mathbb{N}, \tag{3.11}$$

and used the human driver set-up; see Holland (1998) for a review. A shortcoming of these models is that they require no acceleration for zero relative velocity ($\dot{h} = 0$) independent of the distance h. That is, extremely small headways are allowed even when travelling with extremely high speed.

A class of models that managed to eliminate this problem is called the optimal velocity model (OVM),

$$f(h, \dot{h}, v) = \frac{1}{T}(V(h) - v) + W(\dot{h}). \tag{3.12}$$

The first term corresponds to relaxation to a density-dependent optimal velocity given by the increasing function $V(h)$ with a relaxation time T. Clearly, for the human driver set-up, $T = 0$ leads to model (3.9). The increasing function $W(\dot{h})$ shows the dependence on the relative velocity. Notice that one may develop a continuum model like (3.5) from (3.12), but, even for $W = 0$, one obtains $\mathcal{N} \neq 0$ since $\rho = 1/(h + \ell)$ cannot be used in dynamical situations (Berg *et al.* 2000). For $W = 0$, the model has been studied extensively without reaction time (Bando *et al.* 1995; Gasser *et al.* 2004), using human driver set-up

(Davis 2003; Orosz *et al.* 2009) and using robotic driver set-up (Chandler *et al.* 1958; Bando *et al.* 1998; Orosz *et al.* 2010). In this case, the model contains only a few parameters: the relaxation time T, the desired maximum velocity $v_{\max} = \max V(h)$ (attained for large h), the desired stopping distance h_{stop} (below which $V(h) \equiv 0$) and one more parameter corresponding to a desired time gap (that is embedded in V). Despite its simplicity, model (3.12) can reproduce qualitatively almost all kinds of traffic behaviour and also transitions between different behaviours. A shortcoming of the model is that some parameters (like the desired time gap) do not appear explicitly, while others (like the relaxation time T) may be smaller than expected when fitting the model to data (Wagner 2010).

Another car-following model that gained popularity in the last decade was introduced in Treiber *et al.* (2000) and is called the intelligent driver model (IDM),

$$f(h,\dot{h},v) = a\left[1 - \left(\frac{v}{v_{\max}}\right)^4 - \left(\frac{h_{\mathrm{stop}} + v\,T_{\mathrm{gap}} - \dot{h}v/\sqrt{4ab}}{h}\right)^2\right]. \tag{3.13}$$

In this model, all parameters have a clear physical meaning: a is the maximum acceleration, b is the comfortable deceleration, $v_{\max}$ is the desired maximum velocity, h_{stop} is the desired stopping distance and T_{gap} is the desired time gap, and their values are as expected when fitting the model to data (Hoogendoorn & Hoogendoorn 2010). In some situations, the IDM produces unreasonably hard braking behaviour that has recently been eliminated by further adjustments (Kesting *et al.* 2010). Numerous other dynamic models have been developed in the last two decades that are not listed here. We present only those that are simple in form and that we believe had a strong impact on traffic modelling. Note that much more complicated models may be implemented in simulation packages (MITSIM).

There exist a couple of extensions of the car-following models (3.8) and (3.10). In multi-look-ahead models (Herman *et al.* 1959; Wilson *et al.* 2004) drivers respond to the motion of more than one vehicle ahead. Consequently, when monitoring M vehicles in front, the quantities $\sum_{j=0}^{m-1} h_{n+j} + (m-1)\ell = x_{n+m} - x_n - \ell$ and $\sum_{j=0}^{m-1} \dot{h}_{n+j} = v_{n+m} - v_n$, $m = 2,\ldots,M$, also appear in the governing equations (involving reaction times that are usually larger than τ and σ). Notice that, while using the variables h_n, v_n in systems (3.7), (3.8) and (3.7), (3.10), the vehicle length ℓ can be eliminated; this is not possible in the multi-look-ahead case. Such next-nearest neighbour interactions can increase the (linear) stability of uniform flow. There also exist multi-species models (Mason & Woods 1997; Nagatani 2000) where drivers with different characteristics are considered, that is, $g, f, \ell, \tau, \sigma, \kappa \to g_n, f_n, \ell_n, \tau_n, \sigma_n, \kappa_n$ is assumed, which may be different for each n. However, usually only two different species are mixed, corresponding to automobiles and trucks. One might also extend car-following models to make them capable of modelling multi-lane traffic or junctions, in which case lane changes need to be handled (Davis 2004; Kesting *et al.* 2007). Indeed, when a lane change occurs, the right-hand side of model (3.8) or (3.10) changes, that is, one needs to deal with a 'discontinuous dynamical system'.

It is also possible to incorporate stochastic effects to model inconsistencies of driver behaviour and external disturbances (such as the weather or road unevenness). However, in the current literature, this is not typical, except in

cases when the model is discretized in time. It has particular importance when space and velocities are also discretized (besides time), in which case we talk about cellular automata models (Nagel & Schreckenberg 1992). These models used to be very popular because quick realizations of numerical simulations were possible, but the discretization may 'wash away' many dynamical effects that are important for understanding traffic dynamics.

Before concluding this section, we collect the characteristic times appearing in traffic. We would like to emphasize that, even though these are close to each other in magnitude, their physical meaning and their effects on the dynamics may be completely different.

— *Reaction time.* $\tau, \sigma, \kappa \approx$ 0.5–1.5 s is a dead time required to process information about stimuli and to initiate actions. It may be different for different kinds of stimuli; see model (3.10).
— *Relaxation time.* $T \approx$ 1–10 s appears owing to the fact that vehicles are capable of only finite acceleration; see model (3.12).
— *Desired time gap* (*also called time headway*). $T_{\mathrm{gap}} \approx$ 1–2 s is the time distance drivers would like to keep when following a leader; see model (3.13).

We remark that these times should also be distinguished from the numerical update time that is simply an artefact of time discretization. However, depending on the discretization scheme, its effects may be similar to those of the multiples of the reaction time (Kesting & Treiber 2008). In the following sections, all results are presented on the dynamic car-following model (3.7), (3.10), but most methods are also applicable to (3.7), (3.8) and (3.1), (3.4).

4. Traffic in equilibrium

As mentioned above, a traffic model should be able to reproduce uniform flow where both the velocities and the headways are time independent, that is, for identical vehicles, we have

$$h_n(t) \equiv h^*, \quad \dot{h}_n(t) \equiv 0 \quad \text{and} \quad v_n(t) \equiv v^*. \tag{4.1}$$

(For non-identical vehicles, the first formula would become $h_n(t) \equiv h_n^*$, where h_n^* may be different for each vehicle.) We also assume that a functional relationship exists between the equilibrium headway h^* and the equilibrium velocity v^*, that is,

$$0 = f(h^*, 0, v^*) \quad \Rightarrow \quad v^* = V(h^*) \quad \Leftrightarrow \quad h^* = V^{-1}(v^*), \tag{4.2}$$

where V is assumed to have the following properties:

— V is continuous and monotonously increasing (the more sparse traffic is, the faster drivers want to travel).
— $V(h) \equiv 0$ for $h \leq h_{\mathrm{stop}}$ (in very dense traffic, drivers intend to stop).
— $V(h) \equiv v_{\mathrm{max}}$ for large h (in very sparse traffic, drivers intend to drive with maximum speed—often called free flow).

Two examples are shown in figure 3*a*,*b*. The function in figure 3*a* represents that between stopping and free-flow conditions—drivers intend to keep a constant time gap T_{gap}. However, this function is non-smooth, which can complicate the

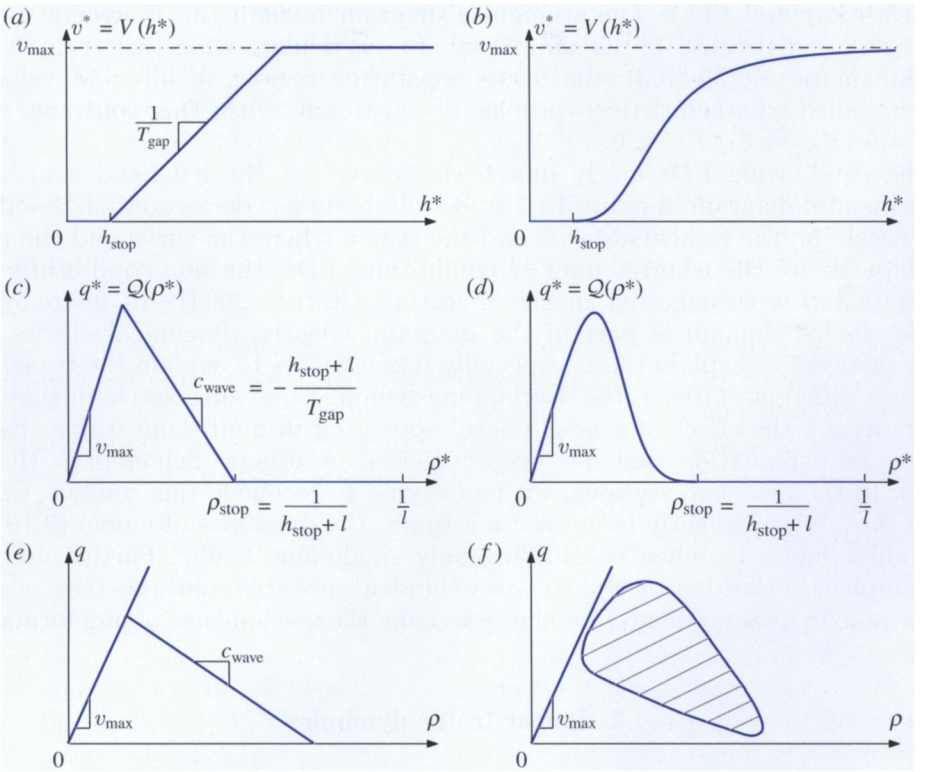

Figure 3. (a,b) Equilibrium speed–density diagrams. (c,d) Equilibrium flux–density (fundamental) diagrams determined from (a,b) by using equation (4.3). (e,f) Non-equilibrium FDs suggested in the literature (see figure 1a).

mathematical analysis of the corresponding models, so in many cases smoothed functions such as the one in figure 3b are used (that usually do not contain T_{gap} explicitly).

Such an equilibrium speed–density function has been explicitly built into the models (3.9) and (3.10), (3.12), where it is often called the optimal velocity function. For (3.10), (3.13), one finds that $V^{-1}(v^*) = (h_{\text{stop}} + v^* T_{\text{gap}})/\sqrt{1-(v^*/v_{\max})^4}$ and the corresponding V is similar in shape to figure 3b—except that $V(h) < 0$ for $h \le h_{\text{stop}}$, i.e. cars intend to reverse in this regime. However, the uniform flow is usually unstable here, and such a non-physical motion is rarely observed in simulations. Notice also that $V'(h_{\text{stop}}) = 1/T_{\text{gap}}$. Finally, we remark that the model (3.10), (3.11) does not admit such a uniform flow equilibrium: assuming $v_n(t) \equiv v^*$, any $h_n(t) \equiv h_n^*$ is possible (where h_n^* may be different for each vehicle, even for identical drivers).

In equilibrium, one may define the equilibrium density and the flux as

$$\rho^* = \frac{1}{h^* + \ell} \quad \text{and} \quad q^* = \rho^* v^* = \frac{V(h^*)}{h^* + \ell} = \rho^* \mathcal{V}(\rho^*) := \mathcal{Q}(\rho^*), \tag{4.3}$$

where $\mathcal{V}(\rho^*) = V(1/\rho^* - \ell)$. This way, the equilibrium speed–headway diagrams in figure 3a,b can be transformed into the equilibrium flux–density (fundamental) diagrams in figure 3c,d. Indeed, the function $\mathcal{V}$ is explicitly built into the

models (3.3) and (3.5). The triangular diagram in figure 3*c* is widely used in the literature because of its simplicity. In particular, when inserting it into the kinematic model (3.3), the fronts separating regions of different velocities (often called characteristics) propagate upstream with the constant speed $c_{\mathrm{wave}} = -(h_{\mathrm{stop}} + \ell)/T_{\mathrm{gap}} < 0$.

The equilibrium FDs nicely match the 'curve' on the left-hand side of the experimental diagram in figure 1*a*, but definitely do not do a good job describing the 'patch' on the right-hand side and the region where the curve and the patch overlap. To fix this shortcoming of equilibrium FDs, the non-equilibrium FDs in figure 3*e*,*f* are suggested in the literature (Kerner 2004)—in figure 3*f*, the whole shaded domain is part of the diagram. Clearly, dynamical effects need to be involved to explain these, especially if one wishes to explain the transitions between different states in the overlapping region. Some authors claim that such diagrams are the effect of a new 'phase' appearing in multi-lane traffic (Kerner 2009)—an explanation that has been criticized by others (Schönhof & Helbing 2009). In the next two sections, without trying to reconcile this conflict, we will show that, for sufficiently large reaction times, the dynamics of model (3.10) can reproduce figure 1*a* when considering only single-lane traffic. Furthermore, we will emphasize that it is useful to study 'hidden' unstable solutions (that are not observable in measurements) for characterizing the mechanisms of jam formation.

5. Linear traffic dynamics

There may be two obvious reasons why the right-hand side of the equilibrium FDs in figure 3*c*,*d* is not observable in empirical data. The equilibria either do not exist or they are not stable (solutions diverge and approach some other state). The latter case may be studied by linearizing model (3.10) about the equilibrium (equation (4.1)). Defining the perturbations $\tilde{h}_n(t) = h_n(t) - h^*$, $\tilde{v}_n(t) = v_n(t) - v^*$, one may obtain the linearized equations

$$\dot{\tilde{v}}_n(t) = F\tilde{h}_n(t-\tau) + G\dot{\tilde{h}}_n(t-\sigma) - H\tilde{v}_n(t-\kappa), \tag{5.1}$$

where the derivatives

$$F = \partial_h f(h^*, 0, v^*), \quad G = \partial_{\dot{h}} f(h^*, 0, v^*) \quad \text{and} \quad H = -\partial_v f(h^*, 0, v^*) \tag{5.2}$$

are assumed to be positive to obtain physically realistic driver behaviour, i.e. drivers intend to decrease the perturbations. Indeed, we have $\tilde{h}_n(t) = \tilde{x}_{n+1}(t) - \tilde{x}_n(t)$, $\dot{\tilde{x}}_n(t) = \tilde{v}_n(t)$ and $\dot{\tilde{h}}_n(t) = \tilde{v}_{n+1}(t) - \tilde{v}_n(t)$ here.

There are (at least) three different methodologies to study the linear stability of the uniform flow (also often called string stability) that are used in the literature and lead to the same results. We named these approaches after the communities that use them the most.

— '*Physicist's approach*'. An infinite road is considered and (without specifying the boundary conditions) the travelling wave ansatz $\tilde{x}_n(t) = \mathrm{Re}(A\,\mathrm{e}^{\lambda t + \mathrm{i}\theta n})$, $\lambda \in \mathbb{C}$, $\theta \in (0, 2\pi)$, is assumed. Indeed, this ansatz is equivalent to performing a Laplace transformation in time and a (discrete)

Fourier transformation in space, and it leads to a second-order equation for λ. To obtain stability, one needs to ensure $\mathrm{Re}(\lambda) < 0$ for all solutions (Bando *et al.* 1995; Wilson 2008).

— '*Dynamical systems approach*'. A circular road configuration (i.e. periodic boundary conditions) is considered such that N vehicles are placed on a ring of length $L + N\ell$ (yielding $h^* = L/N$ and $x_{N+1}(t) \equiv x_1(t)$). Usually, the large N limit is taken: $N \to \infty$ such that L/N is kept constant. The trial solution $\tilde{x}_n(t) = A_n \mathrm{e}^{\lambda t}$, $\lambda, A_n \in \mathbb{C}$, is assumed, which is equivalent to performing a Laplace transformation in time. This leads to a $2N$th-order characteristic equation for λ and again $\mathrm{Re}(\lambda) < 0$ ensures stability (Gasser *et al.* 2004; Orosz *et al.* 2010).

— '*Control engineer's approach*'. A platoon configuration is considered such that the leader's motion can be assigned—in equilibrium, it travels with v^*. Then the $(n+1)$st and the nth vehicles are considered as an input $(\tilde{x}_{n+1})$ output $(\tilde{x}_n)$ system, and a transfer function is determined through a Laplace transformation. The condition for string stability requires the magnitude of the corresponding transfer function to be less than 1 for every excitation frequency (output has to be smaller than input) along the platoon (Ioannou & Xu 1994; Swaroop *et al.* 1994; Zhou & Peng 2005).

Notice that, in the second approach, the key parameter is the equilibrium headway h^*, while, in the third approach, it is the equilibrium velocity v^*. However, these quantities are linked by equation (4.2).

The stability loss occurs for $\lambda = \pm \mathrm{i}\omega$, and travelling waves with frequency $\omega \in \mathbb{R}^+$ appear. In the dynamical system terminology, this kind of stability loss is called a Hopf bifurcation. One may calculate that $A_n = A\,\mathrm{e}^{\mathrm{i}(2k\pi/N)n}$, $k = 1, \ldots, N-1$, and so the small-amplitude waves can be written in the form

$$\tilde{x}_n(t) = A \sin\left(\omega t + \frac{2k\pi}{N} n\right) \quad \Rightarrow \quad \tilde{v}_n(t) = v^{\mathrm{amp}} \cos\left(\omega t + \frac{2k\pi}{N} n\right), \tag{5.3}$$

where $v^{\mathrm{amp}} = A\omega$. This justifies the physicist's ansatz about the spatial patterns and gives $\theta = 2k\pi/N$, $k = 1, \ldots, N-1$. Note that k plays the role of a discrete wavenumber.

In appendix A, the simple case of zero delays is considered. In this case, the characteristic equation has finitely many solutions for λ, and it is easy to prove that all approaches give the same stability condition and that stability is lost to low-frequency, long-wavelength ($k = 1$) oscillations. For non-zero delays, however, the characteristic equation has infinitely many solutions for λ owing to the terms $\mathrm{e}^{-\lambda\tau}, \mathrm{e}^{-\lambda\sigma}, \mathrm{e}^{-\lambda\kappa}$. If the delays are sufficiently large, the flow may lose its stability to high-frequency, short-wavelength ($k \gg 1$) oscillations (Kesting & Treiber 2008; Orosz *et al.* 2010). Choosing even larger delays may lead to situations in which even the drivers' intentions to decrease the transients (expressed by $F, G, H > 0$ in equation (5.1)) fail to work and so the controller becomes unstable (Sipahi & Niculescu 2010). Finally, we remark that the control engineer's approach may allow one to study convective instabilities (Pipes 1953; Ward & Wilson 2010), while the dynamical systems approach is useful if one wishes to analyse the effects of nonlinearities. In the next section, we demonstrate that nonlinearities play an essential role in determining the emergent state of traffic systems.

6. Nonlinear traffic dynamics

The most popular way to study the behaviour of nonlinear traffic models is using numerical simulations. The great advantage of this approach is that almost any extension of model (3.10) can be implemented (non-identical drivers, multi-lane traffic, junctions). In some cases, it is more difficult to write the system in a closed mathematical form than implementing the algorithm for numerical simulations. Still, this approach has drawbacks. It may not be easy to determine the causes of certain behaviours appearing in simulations (especially in regions of multi-stability). This is due to the difficulty in detecting unstable solutions by numerical simulation in such a high-degree-of-freedom system without having some prior knowledge about them. As will be explained below, it is critical to explore such solutions if one wishes to understand the underlying mechanisms of jam formation.

In this section, we consider a single lane with periodic boundary conditions, building the analysis on the dynamical systems approach outlined in the previous section. We show that the qualitative features of the empirical FD in figure 1*a* can be reproduced by a dynamic model (3.10) when considering finite reaction times. For more details about the techniques used and results presented, one may consult Gasser *et al.* (2004), Orosz & Stépán (2006) and Orosz *et al.* (2009). Some claims about multi-stability are also given in Krauss *et al.* (1997), Lee *et al.* (1998), Igarashi *et al.* (2001), Safonov *et al.* (2002) and Helbing & Moussaid (2009) by using different tools.

Here we consider the OVM (3.10), (3.12), but one may reproduce the analysis—and obtain qualitatively similar behaviour—for any dynamic model that admits a uniform flow equilibrium (4.1), (4.2) with an equilibrium function that looks like figure 3*b*; for example, see the IDM (3.10), (3.13) except for small equilibrium headways. We consider the human driver set-up $\tau = \sigma > 0$, $\kappa = 0$ for the reaction times and assume the optimal and relative velocity functions

$$V(h) = v_{\max} \begin{cases} 0, & \text{if} \quad h \in [0,1], \\ \dfrac{((h - h_{\text{stop}})/s)^3}{1 + ((h - h_{\text{stop}})/s)^3}, & \text{if} \quad h \in [1,\infty), \end{cases} \qquad W(\dot{h}) = \beta \dot{h}. \tag{6.1}$$

The function V is shown in figure 3*b*. To decrease the number of parameters, we rescale the distances by the desired stopping distance h_{stop} and rescale the velocities by the desired speed $v_{\max}$. However, to maintain the clarity of presentation, we do not represent this rescaling in the illustrations below. The corresponding dimensionless parameters are fixed as $s/h_{\text{stop}} = 2$, $\ell/h_{\text{stop}} = 1$, $\beta h_{\text{stop}}/v_{\max} = 0.1$, $T v_{\max}/h_{\text{stop}} = 2$, $\tau v_{\max}/h_{\text{stop}} = 2$. Thus, the only free parameter left in the model (3.10), (3.12), (6.1) is the equilibrium headway $h^* = L/N$, and we show the qualitative changes in the dynamics when this parameter is varied. The results are given for $N = 33$, which is small enough to reveal the detailed microscopic dynamics but large enough to approximate the $N \to \infty$ case well.

First, the results of the linear stability investigations are shown. Considering the linearization (5.1), one obtains $F = V'(h^*)/T$, $G = \beta$, $H = 1/T$. The algebraic expressions for the stability boundaries are fairly complicated for $\tau > 0$, and they are not shown here. However, the stability criterion is qualitatively similar

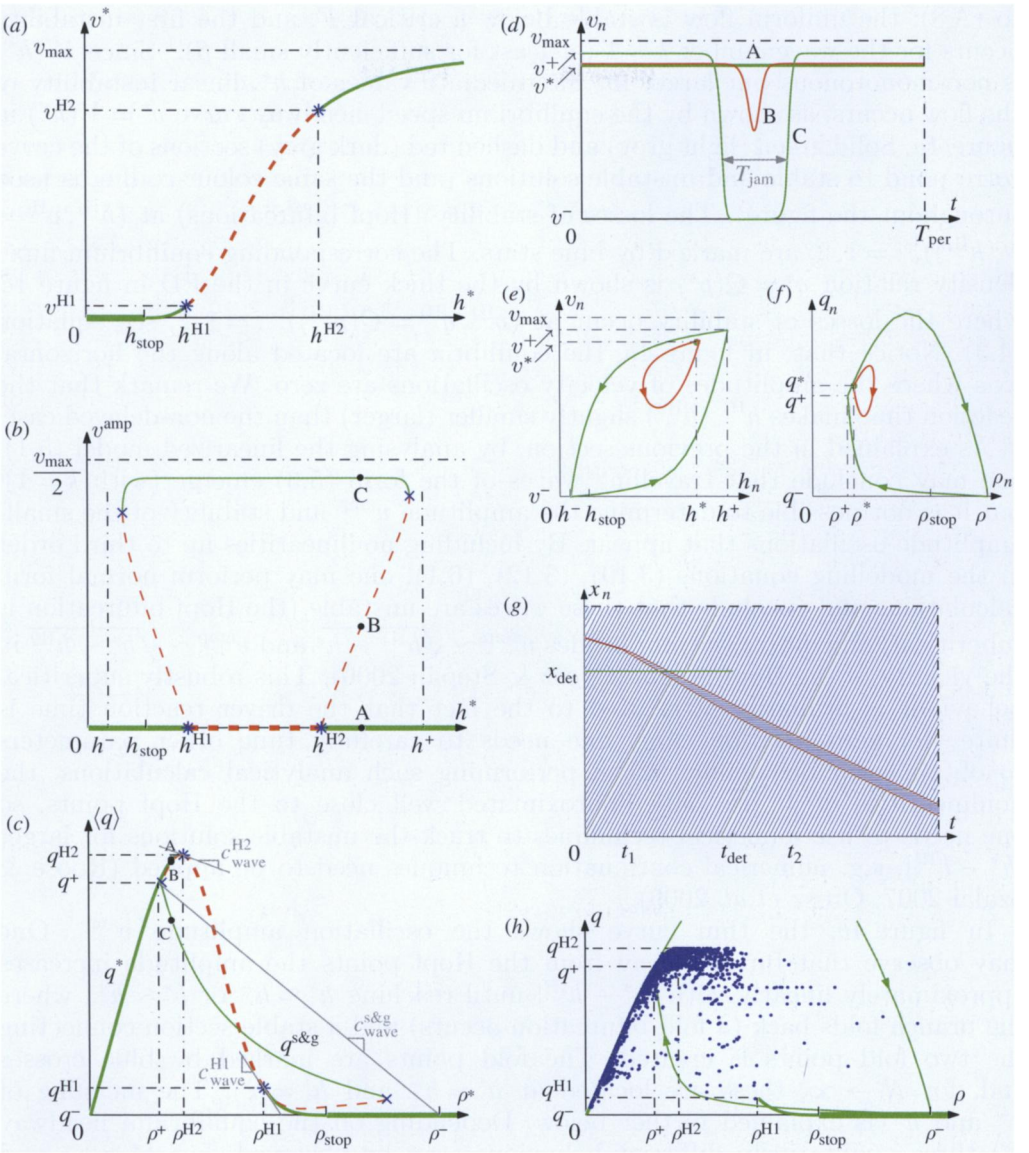

Figure 4. Stable and unstable solutions in traffic represented by green (light grey) and red (dark grey) curves, respectively. (*a–c*) Bifurcation diagrams showing the qualitative changes in dynamics when the equilibrium headway h^* (or the equilibrium density ρ^*) is varied. Thick curves represent uniform flow equilibria while thin curves represent travelling waves. Stability changes are denoted by blue stars for equilibria (Hopf bifurcations) and by blue crosses for travelling waves (fold bifurcations). (*d–f*) Stable and unstable solutions in time and in state space corresponding to the points A, B and C in (*b*,*c*). (*g*) Development of stop-and-go oscillations triggered by an over-the-threshold perturbation. Each curve represents the motion of a particular vehicle and the backward-propagating stop-front and go-front are highlighted in red. (*h*) FD diagram with data collected for different values of ρ^* at the cross section $x = x_{\mathrm{det}}$ during the time interval $t \in [0, t_{\mathrm{det}}]$.

to (A 8): the uniform flow is stable below a critical F, and the first instability occurs for the wavenumber $k=1$ (at least for sufficiently small β).[1] Since $V'(h^*)$ is non-monotonous but larger for intermediate values of h^*, linear instability of the flow occurs, as shown by the equilibrium speed–headway curve $v^*=V(h^*)$ in figure 4*a*. Solid green (light grey) and dashed red (dark grey) sections of the curve correspond to stable and unstable solutions (and the same colour-coding is used throughout the figure). The losses of stability (Hopf bifurcations) at $(h^{\mathrm{H}i}, v^{\mathrm{H}i}=V(h^{\mathrm{H}i}))$, $i=1,2$, are marked by blue stars. The corresponding equilibrium flux–density relation $q^*=Q(\rho^*)$ is shown by the thick curve in the FD in figure 4*c*, where the losses of stability occur at $(\rho^{\mathrm{H}i}, q^{\mathrm{H}i}=Q(\rho^{\mathrm{H}i}))$, $i=1,2$; see equation (4.3). Notice that, in figure 4*b*, the equilibria are located along the horizontal axis where the amplitudes of velocity oscillations are zero. We remark that the reaction time makes h^{H1} (h^{H2}) slightly smaller (larger) than the non-delayed case.

As explained in the previous section, by analysing the linearized model (5.1), one may conclude that travelling waves of the form (5.3) emerge (with $k=1$), but it is not possible to determine the amplitude v^{amp} and stability of the small-amplitude oscillations that appear. By including nonlinearities up to third order in the modelling equations (3.10), (3.12), (6.1), one may perform normal form calculations and conclude that these waves are unstable (the Hopf bifurcation is subcritical) and derive the amplitudes $v^{\mathrm{amp}}\sim\sqrt{h^{\mathrm{H1}}-h^*}$ and $v^{\mathrm{amp}}\sim\sqrt{h^*-h^{\mathrm{H2}}}$ in the vicinity of the Hopf points (Orosz & Stépán 2006). This robustly subcritical behaviour is primarily attributed to the fact that the driver reaction time is finite—for zero reaction time, one needs to carefully tune other parameters to obtain such behaviour. When performing such analytical calculations, the nonlinearities of V are only approximated well close to the Hopf points, so one needs to use numerical techniques to track the unstable solutions for larger $|h^*-h^{\mathrm{H}i}|$, e.g. numerical continuation techniques need to be applied (Roose & Szalai 2007; Orosz *et al.* 2009).

In figure 4*b*, the thin curve shows the oscillation amplitude v^{amp}. One may observe that further away from the Hopf points the amplitude increases approximately linearly with $|h^*-h^{\mathrm{H}i}|$ until reaching $h^*\approx h^-$ or $h^*\approx h^+$, where the branch folds back (a fold bifurcation occurs) and a stable section connecting the two fold points is created. The fold points are marked by blue crosses and, for $N\to\infty$, these are located at $h^*=h^-$ and $h^*=h^+$. The meaning of h^- and h^+ is explained further below. Depending on the equilibrium headway h^*, three qualitatively different behaviours can be observed. For $h^*<h^-$ and $h^*>h^+$, the only stable solution is the linearly stable equilibrium, which is, consequently, globally stable. For $h^{\mathrm{H1}}<h^*<h^{\mathrm{H2}}$, the equilibrium is unstable, and the only stable solution is the large-amplitude oscillatory solution. Finally, for $h^-<h^*<h^{\mathrm{H1}}$ and $h^{\mathrm{H2}}<h^*<h^+$, both the equilibrium and the large-amplitude oscillatory solution are stable (bistability occurs), and their basins of attraction are separated by the unstable oscillatory solution. It is important to remark that h^- (h^+) increases (decreases) with the reaction time and, consequently, the bistable domains (h^-, h^{H1}) and (h^{H2}, h^+) become much more extended than the non-delayed case.

[1]We remark that the wavenumbers $k>1$ may also have important roles (Orosz *et al.* 2009, 2010), but those are not discussed here in detail.

Before explaining how to represent the oscillatory branches on the FD, we describe the oscillatory solutions in more detail. In figure 4*b*, we marked the points A, B and C along the branches in the bistable regime $h^{\mathrm{H2}} < h^* < h^+$ (at $h^*/h_{\mathrm{stop}} = 4.7$) and show the corresponding velocity profiles $v_n(t)$ in figure 4*d*. Indeed, the velocity is constant for the equilibrium (A) but changes periodically for oscillations (B and C). The time profiles are shown for a chosen vehicle, but they look identical for all other vehicles except for a time shift: for two consecutive vehicles, $v_n(t) = v_{n+1}(t - T_{\mathrm{per}}/N)$, where T_{per} is the period, which is almost the same for the stable and unstable oscillations. These are, indeed, travelling waves, but they are not approximated well by harmonic oscillations anymore; see equation (5.3) for $k = 1$, where $T_{\mathrm{per}} = 2\pi/\omega$. For the unstable oscillatory solution, the velocity only changes in a short time interval: the driver taps on the brake. For the stable oscillatory solution, high- and low-velocity plateaux appear that are connected by a stop-front (where the velocity drops) and a go-front (where the velocity rises): these are the well-known stop-and-go waves.

The corresponding trajectories are shown in the state space (h_n, v_n) in figure 4*e*, where the points (h^*, v^*), (h^+, v^+) and (h^-, v^-) are marked. The first point is the uniform flow equilibrium where $v^* = V(h^*)$; see equations (4.1), (4.2). The latter two points we call semiequilibria because along the stable oscillations vehicles stay in one of these states most of the time (figure 4*d*) and, consequently, at a chosen time instant, most vehicles are in one of these equilibria. One may find that, for quasi-equilibria,

$$v^{\pm} \approx V(h^{\pm}) \tag{6.2}$$

is true (see equation (4.2)). We remark that it is not known how to determine $h^{\pm}$ analytically for a given car-following model. One may also plot the oscillations by using the 'Lagrangian density' $\rho_n = 1/(h_n + \ell)$ and 'Lagrangian flux' $q_n = \rho_n v_n$, as shown in figure 4*f*. Here, the equilibrium is located at (ρ^*, q^*), whereas the quasi-equilibria are located at (ρ^+, q^+) and (ρ^-, q^-), where

$$\rho^{\pm} = \frac{1}{h^{\pm} + \ell} \quad \text{and} \quad q^{\pm} = \rho^{\pm} v^{\pm} \approx \mathcal{Q}(\rho^{\pm}); \tag{6.3}$$

see equations (4.3) and (6.2).

In the bistable regimes, the system may approach the equilibrium or the stop-and-go oscillation depending on the initial conditions. The role of the unstable oscillation is that it separates the basins of attractions of the two stable states. In other words, it determines the threshold for the strength of perturbations necessary to 'transfer' the systems from uniform flow to stop-and-go motion. Over-the-threshold localized perturbations may trigger stop-and-go jams even when the uniform flow is linearly stable. Figure 4*g* shows the vehicles' trajectories in space–time when the system is initialized in equilibrium, except one driver whose velocity and headway is reduced ($h^*/h_{\mathrm{stop}} = 4.7$, as in figure 4*d–f*). This finite perturbation is chosen to be over-the-threshold, and consequently it is amplified when propagating upstream, leading to stop-and-go oscillation. The stop-front (where the velocity drops) and the go-front (where the velocity rises)

are highlighted in red. During the formation of the stop-and-go wave, there are three different characteristic wave speeds observable:

— The wave speed corresponding to the linear stability loss at the Hopf points. This may be calculated from equations (5.3), (A 7), (A 8) because the delay does not alter the expression in the large N limit ($k=1, N\to\infty \Rightarrow k/N\to 0$). Thus, one may obtain

$$c_{\mathrm{wave}}^{\mathrm{H}i} = v^{\mathrm{H}i} - (h^{\mathrm{H}i}+\ell)\frac{F^{\mathrm{H}i}}{H^{\mathrm{H}i}}, \quad i=1,2, \tag{6.4}$$

where $F^{\mathrm{H}i}=\partial_h f(h^{\mathrm{H}i},0,v^{\mathrm{H}i})$ and $H^{\mathrm{H}i}=-\partial_v f(h^{\mathrm{H}i},0,v^{\mathrm{H}i})$; see equation (5.2). For the OVM (3.10), (3.12), (6.1), we have $F^{\mathrm{H}i}/H^{\mathrm{H}i}=V'(h^{\mathrm{H}i})$, which yields

$$c_{\mathrm{wave}}^{\mathrm{H}i} = v^{\mathrm{H}i} - (h^{\mathrm{H}i}+\ell)\,V'(h^{\mathrm{H}i}) = \mathcal{Q}'(\rho^{\mathrm{H}i}), \quad i=1,2. \tag{6.5}$$

This approximates the wave speed in figure 4*g* for $t\lesssim t_1$ (for $i=2$), because h^* is quite close to $h^{\mathrm{H}2}$.

— The wave speed of the developing stop-and-go wave ($t_1\lesssim t\lesssim t_2$ in figure 4*g*). In this case, the speed of the stop-front (where vehicles enter the jam) and the go-front (where they leave the jam) is different and may be determined by adding higher order corrections in k/N to equation (6.4) (Ward & Wilson 2010).

— The wave speed of the fully developed stop-and-go wave ($t\gtrsim t_2$ in figure 4*g*). This is very well approximated by

$$c_{\mathrm{wave}}^{\mathrm{s\&g}} = \frac{h^+v^- - h^-v^+ + \ell(v^- - v^+)}{h^+ - h^-} = \frac{q^+ - q^-}{\rho^+ - \rho^-} < 0, \tag{6.6}$$

which may be obtained from wave kinematics (Lighthill & Whitham 1955).

When studying the oscillations for different values of h^*, one may observe that unstable solutions for $h^{\mathrm{H}2} < h^* < h^+$ are similar in shape to those shown in figure 4*d–f*, but their minima decrease as h^* approaches h^+. For $h^- < h^* < h^{\mathrm{H}1}$, the unstable solutions look like the unstable solutions in figure 4*d* but upside-down, and now the maxima increase as h^* approaches h^-. On the other hand, one may find that the stable stop-and-go solution for $h^- < h^* < h^+$ almost does not change in state space compared with figure 4*e*,*f*, but the lengths of low- and high-velocity plateaux change compared with figure 4*d* according to

$$\frac{T_{\mathrm{jam}}}{T_{\mathrm{per}}} \approx \frac{h^+ - h^*}{h^+ - h^-}. \tag{6.7}$$

(Here T_{jam} is measured at $v_n = v_{\max}/3$.) In other words, h^+ and h^- are independent of the equilibrium density h^*, and, in fact, the fold bifurcations happen in figure 4*b* when the low- and high-velocity plateaux disappear at $h^*\approx h^+$ and $h^*\approx h^-$, respectively.

To approximate the flow along the oscillatory branch, we averaged the Lagrangian flux $q_n = \rho_n v_n$ for one period and plotted the average $\langle q \rangle$ as a function of equilibrium density ρ^* in figure 4*c*. For equilibria, $\langle q \rangle = q^*$, while, for the stop-and-go oscillations, one may use equation (6.7) and obtain

$$\langle q \rangle \approx q^- \frac{h^+ - h^*}{h^+ - h^-} + q^+ \frac{h^* - h^-}{h^+ - h^-} := q^{\mathrm{s\&g}}, \tag{6.8}$$

which is a good approximation except close to the fold points. Notice that the wave speed (6.5) gives the gradients of the equilibrium curve $q^* = \mathcal{Q}(\rho^*)$ at the Hopf points $(\rho^{\mathrm{H}i}, q^{\mathrm{H}i})$, $i = 1, 2$, while the wave speed (6.6) gives the gradient of the line connecting points (ρ^+, q^+) and (ρ^-, q^-). Clearly, this line does not coincide with $q^{\mathrm{s\&g}}$ (in contrast to the suggestion in figure 1*e*). In the FD in figure 4*c*, the bistable regimes are located at $\rho^+ < \rho^* < \rho^{\mathrm{H2}}$ and $\rho^{\mathrm{H1}} < \rho^* < \rho^-$. Notice that $h^- < h_{\mathrm{stop}} \Leftrightarrow \rho^- > \rho_{\mathrm{stop}}$, that is, during oscillations, higher densities can be observed than suggested by the equilibrium FD. This corresponds to the fact that drivers intend to stop at the distance h_{stop}, but can only achieve this at the distance h^- owing to their inertia and reaction time.

As mentioned above, if the reaction times were omitted, the Hopf bifurcations are usually supercritical (or weakly subcritical), which would result in $(\rho^{\mathrm{H2}}, q^{\mathrm{H2}}) \approx (\rho^+, q^+)$ and $(\rho^{\mathrm{H1}}, q^{\mathrm{H1}}) \approx (\rho^-, q^-)$ and would also yield $c^{\mathrm{H}i}_{\mathrm{wave}} \approx c^{\mathrm{s\&g}}_{\mathrm{wave}}$; see (6.5), (6.6). In this case, the extended bistable regions would disappear, oscillation would appear only for $\rho^{\mathrm{H2}} \lesssim \rho^* \lesssim \rho^{\mathrm{H1}}$ and the corresponding FD would be similar to figure 3*d*. That is, no overlapping region between equilibria and oscillations could be observed, which contradicts the empirical findings in figure 1*a*.

When measuring 'Eulerian density' and 'Eulerian flux' at a cross section, one may record density–flux combinations along the stable part of the equilibrium branch in figure 4*c* or in the area enclosed by the stable orbit in figure 4*f*; recall that the shape of this orbit practically does not change for $\rho^+ < \rho^* < \rho^-$. The enclosed area may be filled owing to transients, that is, owing to transitions between the equilibrium and the stop-and-go oscillations. Figure 4*h* depicts the flux–density data collected at $x = x_{\mathrm{det}}$ (that is upstream from the localized perturbation) during the time interval $t \in [0, t_{\mathrm{det}}]$ for different values of the equilibrium density $\rho^* < \rho^{\mathrm{H1}}$ and different perturbation sizes. Similar to empirical studies, we recorded the velocity of vehicles when passing the detector and the time elapsed between passings, and, from these, we calculated the flux and density. As expected, the data points either lie in the vicinity of the equilibrium branch or are enclosed by the stable orbit. The rest of the enclosed domain is rarely observed when recording Eulerian data (e.g. one never records zero flux), but is accessible when collecting Lagrangian data. The recorded data correspond well to the empirical data shown in figure 1*a* and, what is more, we now have a clear dynamical explanation for its qualitative features.

In the single-lane models studied above, traffic jams may be triggered by sufficiently large irregularities in driver behaviour, which may be due to lack of concentration, aggressive or timid driving, uphill segments or any other unexpected manoeuvres of neighbouring vehicles. However, for multi-lane traffic (that may include on- and off-ramps), the lanes are also coupled to each other by the lane changes, so the motion of vehicles in one lane may also trigger traffic jams in the neighbouring lane. That is, the excitable dynamics, which is rooted

in the nonlinear longitudinal dynamics of single-lane traffic, may become more pronounced for multi-lane configurations. Moreover, in many cases, stop-and-go jams emanate from bottlenecks, regions of the highway where the maximum flux is reduced, e.g. by road works or lane closure (Kerner 2008). Apart from triggering stop-and-go waves, the bottleneck usually results in a standing wave, that is, a localized jam forms at the bottleneck. The dynamical interaction between these standing and travelling waves may lead to intricate patterns such as those shown in Gasser & Werner (2010), where the results are presented from both microscopic and macroscopic perspectives. Indeed, the above dynamical principles need to be respected when one wishes to eliminate congestion by controlling traffic.

7. Traffic control

Traffic control existed even before automobiles appeared, in particular in big cities. For example, archaeological evidence has been found for traffic planning in the ancient Roman city of Pompeii (Powell & Poehler 2008), while the first traffic signal was installed two millennia later in 1868 in the city of London, UK (Mueller 1970). However, the importance of control has been increasing with the growing number of motor vehicles. Besides using traffic lights, one may introduce ramp metering and bridge/tunnel tolls to increase the efficiency of road networks (Varaiya 2008). To review all possibilities of traffic management is far beyond the scope of this introductory paper, so here we rather focus on the state-of-the-art scientific methods that may help to improve the efficiency of the current infrastructure.

When designing flow control algorithms, it is beneficial to view traffic at the macroscopic level (Luspay *et al.* 2010). On highways, the goal is to keep the traffic near the free-flow condition by controlling the in- and outflow on the on- and off-ramps and by assigning the velocity with the help of variable message signs (Carlson *et al.* 2010). When implementing such control strategies, usually the equilibrium FD in figure 3*a* is used and the system is kept on the left-hand side of the maximum (Kurzhanskiy & Varaiya 2010). On the other hand, one may use non-equilibrium FDs, like those in figure 4*c*,*h*, and try to keep the system on the equilibrium branch even in the overlapping region—this would allow higher flux, that is, higher efficiency. One can also investigate the macroscopic dynamics of urban networks where flow control is mostly managed by pre-programmed or adaptive traffic lights. For example, using the FD in figure 3*a* for road sections between traffic lights, one may determine 'integrated' FDs for the whole network and study the effects of different route planning and signalling strategies (Daganzo & Geroliminis 2008; Helbing 2009; Mazloumian *et al.* 2010).

Emerging information technologies may also be exploited for controlling traffic at the microscopic level. In particular, ACC devices consist of a radar that measures the distance and velocity difference from the driver in front, an on-board computer that calculates the required action (braking or acceleration) according to a driving rule like model (3.10) and actuators that carry out the required actions. Originally, such systems were designed to increase the driver's comfort (Swaroop *et al.* 1994; Ioannou & Xu 1994) and the design is based on linear systems theory. When designing the next generation of controllers, one needs to

consider nonlinearities (that are primarily imposed by the nonlinearities of the speed–headway functions such as those in figure 3*a*,*b*), and also the effects of time delays (Kesting & Treiber 2008; Orosz *et al.* 2010).

Even though some vehicles are already equipped with such devices, one cannot expect that all cars will have ACCs in the foreseeable future. For this reason, it is important to design controllers with characteristics similar to human drivers and to study situations where human-driven and autonomous vehicles are mixed. Recent results show that even small percentages of ACC-driven vehicles may be beneficial for avoiding congestion (Zhang & Ioannou 2006; Kesting *et al.* 2010). It is expected that microscopic control strategies will enter highways first, but later they may become very important in city traffic as well.

The last DARPA Grand Challenge vindicated that even completely autonomous driving was possible in complex urban environments (Campbell *et al.* 2010). During this competition, vehicles had to obey traffic rules and had to interact with each other and with human-driven vehicles by giving way at intersections and executing overtaking manoeuvres. That is, much more complex situations had to be handled than simple car-following, but vehicles had much more time to process information than in a real traffic situation. 'Speeding up' such autonomous solutions is one of the greatest future challenges in the field. The final goal is indeed to integrate the microscopic and macroscopic control strategies to create intelligent traffic systems of high efficiency.

We gratefully acknowledge the valuable advice and support of Freeman Dyson, FRS. G.O. would like to thank Francesco Bullo, Jeff Moehlis and Róbert Vértesi for helpful discussions and useful comments. We wish to express our appreciation for the assistance received from Suzanne Abbott while compiling this Theme Issue.

Appendix A. Stability of dynamic car-following models without delay

Here, we provide some technical details about the stability analysis of equation (5.1) in the special case $\tau=\sigma=\kappa=0$ in order to demonstrate the different approaches listed in §5. Substituting $\tilde{h}_n(t)=\tilde{x}_{n+1}(t)-\tilde{x}_n(t)$ and $\dot{\tilde{x}}_n(t)=\tilde{v}_n(t)$ into equation (5.1), one obtains

$$\ddot{\tilde{x}}_n(t)+(G+H)\dot{\tilde{x}}_n(t)+F\tilde{x}_n(t)=G\dot{\tilde{x}}_{n+1}(t)+F\tilde{x}_{n+1}(t). \tag{A 1}$$

Assuming $\tilde{x}_n(t)=\mathrm{Re}(A\,\mathrm{e}^{\lambda t+\mathrm{i}\theta n})$, $0<\theta<2\pi$, leads to the equation

$$\lambda^2+(G+H)\lambda+F=(G\lambda+F)\mathrm{e}^{\mathrm{i}\theta}, \tag{A 2}$$

while, using the trial solution $\tilde{x}_n(t)=A_n\mathrm{e}^{\lambda t}$, the characteristic equation

$$(\lambda^2+(G+H)\lambda+F)^N=(G\lambda+F)^N \tag{A 3}$$

is obtained. Taking the Nth root of equation (A 3) results in equation (A 2) with

$$\theta=\frac{2k\pi}{N},\quad k=1,\ldots,N-1. \tag{A 4}$$

Now, by substituting

$$\lambda = \mathrm{i}\omega, \quad \omega \in \mathbb{R}^+, \tag{A 5}$$

into equation (A 2), separating the real and imaginary parts and eliminating ω, one may determine that stability changes (Hopf bifurcations) occur for

$$F = \frac{1}{2}(2G + H)\left[(2G + H)\tan^2\left(\frac{k\pi}{N}\right) + H\right], \tag{A 6}$$

with frequency

$$\omega = (2G + H)\tan\left(\frac{k\pi}{N}\right). \tag{A 7}$$

Note that (for zero delays) only the boundaries $k \leq N/2$ appear in the physically realistic $F, G, H > 0$ parameter regime. It can also be shown that, crossing such a boundary from smaller to larger F, the complex conjugate pair of characteristic roots $\pm\mathrm{i}\omega$ crosses the imaginary axis from left to right, i.e. the system becomes 'more unstable'. Consequently, the stability loss occurs for the lowest wavenumber $k = 1$, and, for $N \to \infty$, the stability condition becomes

$$F < \tfrac{1}{2}(2G + H)H, \tag{A 8}$$

with frequency $\omega \to 0$.

On the other hand, one may simply take the Laplace transform of equation (A 1) and obtain

$$\chi_n(\lambda) = \mathcal{T}(\lambda)\chi_{n+1}(\lambda) \quad \text{and} \quad \mathcal{T}(\lambda) = \frac{G\lambda + F}{\lambda^2 + (G + H)\lambda + F}, \tag{A 9}$$

where $\chi_n(\lambda)$ is the Laplace transform of $\tilde{x}_n(t)$ and $\mathcal{T}(\lambda)$ is the transfer function. Here, one may study the stability of the controller: the poles of $\mathcal{T}(\lambda)$ have to be on the left half complex plane that is ensured by $F, G, H > 0$. On the other hand, to obtain string stability (decay of perturbations from vehicle to vehicle as going along the chain), the inequality $|\mathcal{T}(\mathrm{i}\omega)| < 1$ needs to be satisfied for all $\omega \in \mathbb{R}^+$, that is,

$$F < \tfrac{1}{2}(2G + H)H + \tfrac{1}{2}\omega^2 \tag{A 10}$$

for all $\omega \in \mathbb{R}^+$. The right-hand side of (A 10) is minimal for $\omega \to 0$, yielding (A 8) as a condition for string stability. Notice that substituting the dispersion relation (A 7) into (A 6) results in (A 10), showing that the different approaches are equivalent.

References

Aw, A. & Rascle, M. 2000 Resurrection of 'second order' models of traffic flow. *SIAM J. Appl. Math.* **60**, 916–938. (doi:10.1137/S0036139997332099)

Bando, M., Hasebe, K., Nakayama, A., Shibata, A. & Sugiyama, Y. 1995 Dynamical model of traffic congestion and numerical simulation. *Phys. Rev. E* **51**, 1035–1042. (doi:10.1103/PhysRevE.51.1035)

Bando, M., Hasebe, K., Nakanishi, K. & Nakayama, A. 1998 Analysis of optimal velocity model with explicit delay. *Phys. Rev. E* **58**, 5429–5435. (doi:10.1103/PhysRevE.58.5429)

Benzoni-Gavage, S. & Colombo, R. M. 2003 An n-populations model for traffic flow. *Eur. J. Appl. Math.* **14**, 587–612. (doi:10.1017/S0956792503005266)
Berg, P., Mason, A. D. & Woods, A. W. 2000 Continuum approach to car-following models. *Phys. Rev. E* **61**, 1056–1066. (doi:10.1103/PhysRevE.61.1056)
Campbell, M., Egerstedt, M., How, J. P. & Murray, R. M. 2010 Autonomous driving in urban environments: approaches, lessons and challenges. *Phil. Trans. R. Soc. A* **368**, 4649–4672. (doi:10.1098/rsta.2010.0110)
Carlson, R. C., Papamichail, I., Papageorgiou, M. & Messmer, A. 2010 Optimal motorway traffic flow control involving variable speed limits and ramp metering. *Transport. Sci.* **44**, 238–253. (doi:10.1287/trsc.1090.0314)
Chandler, R. E., Herman, R. & Montroll, E. W. 1958 Traffic dynamics: studies in car following. *Oper. Res.* **6**, 165–184. (doi:10.1287/opre.6.2.165)
Daganzo, C. F. 1995 Requiem for second-order fluid approximations of traffic flow. *Transport. Res. B* **29**, 277–286. (doi:10.1016/0191-2615(95)00007-Z)
Daganzo, C. F. 2002*a* A behavioral theory of multi-lane traffic flow. Part I. Long homogeneous freeway sections. *Transport. Res. B* **36**, 131–158. (doi:10.1016/S0191-2615(00)00042-4)
Daganzo, C. F. 2002*b* A behavioral theory of multi-lane traffic flow. Part II. Merges and the onset of congestion. *Transport. Res. B* **36**, 159–169. (doi:10.1016/S0191-2615(00)00043-6)
Daganzo, C. F. & Geroliminis, N. 2008 An analytical approximation for the macroscopic fundamental diagram of urban traffic. *Transport. Res. B* **42**, 771–781. (doi:10.1016/j.trb.2008.06.008)
Davis, L. C. 2003 Modification of the optimal velocity traffic model to include delay due to driver reaction time. *Physica A* **319**, 557–567. (doi:10.1016/S0378-4371(02)01457-7)
Davis, L. C. 2004 Multilane simulations of traffic phases. *Phys. Rev. E* **69**, 016 108. (doi:10.1103/PhysRevE.69.016108)
Dyson, F. 2004 A meeting with Enrico Fermi—how one intuitive physicist rescued a team from fruitless research. *Nature* **427**, 297–297. (doi:10.1038/427297a)
Gasser, I. & Werner, B. 2010 Dynamical phenomena induced by bottleneck. *Phil. Trans. R. Soc. A* **368**, 4543–4562. (doi:10.1098/rsta.2010.0118)
Gasser, I., Sirito, G. & Werner, B. 2004 Bifurcation analysis of a class of 'car-following' traffic models. *Physica D* **197**, 222–241. (doi:10.1016/j.physd.2004.07.008)
Gazis, D. C., Herman, R. & Rothery, R. W. 1961 Nonlinear follow-the-leader models of traffic flow. *Oper. Res.* **9**, 545–567. (doi:10.1287/opre.9.4.545)
Gipps, P. G. 1981 A behavioural car-following model for computer simulation. *Transport. Res. B* **15**, 105–111. (doi:10.1016/0191-2615(81)90037-0)
Greenshields, B. D. 1935 A study of highway capacity. In *Proc. of the 14th Annual Meeting of the Highway Research Board, Washington, DC*, pp. 448–477.
Greenshields, B. D. 1936 Studying traffic capacity by new methods. *J. Appl. Psychol.* **20**, 353–358. (doi:10.1037/h0063672)
Helbing, D. 1995 Theoretical foundation of macroscopic traffic models. *Physica A* **219**, 375–390. (doi:10.1016/0378-4371(95)00174-6)
Helbing, D. 2001 Traffic and related self-driven many-particle systems. *Rev. Mod. Phys.* **73**, 1067–1141. (doi:10.1103/RevModPhys.73.1067)
Helbing, D. 2009 Derivation of a fundamental diagram for urban traffic flow. *Eur. Phys. J. B* **70**, 229–241. (doi:10.1140/epjb/e2009-00093-7)
Helbing, D. & Moussaid, M. 2009 Analytical calculation of critical perturbation amplitudes and critical densities by non-linear stability analysis of a simple traffic flow model. *Eur. Phys. J. B* **69**, 571–581. (doi:10.1140/epjb/e2009-00042-6)
Herman, R., Montroll, E. W., Potts, R. B. & Rothery, R. W. 1959 Traffic dynamics: analysis of stability in car following. *Oper. Res.* **7**, 86–106. (doi:10.1287/opre.7.1.86)
Highways Agency, UK. See http://www.highways.gov.uk/.
Holland, E. N. 1998 A generalized stability criterion for motorway traffic. *Transport. Res. B* **32**, 141–154. (doi:10.1016/S0191-2615(97)00021-0)
Hoogendoorn, S. & Hoogendoorn, R. 2010 Calibration of microscopic traffic-flow models using multiple data sources. *Phil. Trans. R. Soc. A* **368**, 4497–4517. (doi:10.1098/rsta.2010.0189)

Igarashi, Y., Itoh, K., Nakanishi, K., Ogura, K. & Yokokawa, K. 2001 Bifurcation phenomena in the optimal velocity model for traffic flow. *Phys. Rev. E* **64**, 047102. (doi:10.1103/PhysRevE.64.047102)

Ioannou, P. A. & Xu, Z. 1994 Throttle and brake control systems for automatic vehicle following. *J. Intell. Transport. Syst.* **1**, 345–377. (doi:10.1080/10248079408903805)

Kerner, B. S. 2004 *The physics of traffic: empirical freeway pattern features, engineering applications, and theory.* Understanding Complex Systems. Berlin, Germany: Springer.

Kerner, B. S. 2008 A theory of traffic congestion at heavy bottlenecks. *J. Phys. A* **41**, 215101. (doi:10.1088/1751-8113/41/21/215101)

Kerner, B. S. 2009 *Introduction to modern traffic flow theory and control: the long road to three-phase traffic theory.* Berlin, Germany: Springer.

Kerner, B. S. & Konhäuser, P. 1994 Structure and parameters of clusters in traffic flow. *Phys. Rev. E* **50**, 54–83. (doi:10.1103/PhysRevE.50.54)

Kesting, A. & Treiber, M. 2008 How reaction time, update time, and adaptation time influence the stability of traffic flow. *Comput. Aided Civil Infrastruct. Eng.* **23**, 125–137. (doi:10.1111/j.1467-8667.2007.00529.x)

Kesting, A., Treiber, M. & Helbing, D. 2007 General lane-changing model MOBIL for car-following models. *Transport. Res. Rec.* **1999**, 86–94. (doi:10.3141/1999-10)

Kesting, A., Treiber, M. & Helbing, D. 2010 Enhanced intelligent driver model to access the impact of driving strategies on traffic capacity. *Phil. Trans. R. Soc. A* **368**, 4585–4605. (doi:10.1098/rsta.2010.0084)

Kometani, E. & Sasaki, T. 1958 On the stability of traffic flow. *J. Oper. Res. Soc. Jap.* **2**, 11–26.

Krauss, S., Wagner, P. & Gawron, C. 1997 Metastable states in a microscopic model of traffic flow. *Phys. Rev. E* **55**, 5597–5602. (doi:10.1103/PhysRevE.55.5597)

Kurzhanskiy, A. A. & Varaiya, P. 2010 Active traffic management on road networks: a macroscopic approach. *Phil. Trans. R. Soc. A* **368**, 4607–4626. (doi:10.1098/rsta.2010.0185)

Laval, J. A. & Leclercq, L. 2010 A mechanism to describe the formation and propagation of stop-and-go waves in congested freeway traffic. *Phil. Trans. R. Soc. A* **368**, 4519–4541. (doi:10.1098/rsta.2010.0138)

Lee, H. Y., Lee, H.-W. & Kim, D. 1998 Origin of synchronized traffic flow on highways and its dynamic phase transitions. *Phys. Rev. Lett.* **81**, 1130–1133. (doi:10.1103/PhysRevLett.81.1130)

Lighthill, M. J. & Whitham, G. B. 1955 On kinematic waves. II. A theory of traffic flow on long crowded roads. *Proc. R. Soc. Lond. A* **229**, 317–345. (doi:10.1098/rspa.1955.0089)

Luspay, T. Kulcsàr, B., Varga, I. & Bokor, J. 2010 Parameter-dependent modeling of freeway traffic flow. *Transport Res. C* **18**, 471–488. (doi:10.1016/j.trc.2009.09.005)

Mason, A. D. & Woods, A. W. 1997 Car-following model of multispecies systems of road traffic. *Phys. Rev. E* **55**, 2203–2214. (doi:10.1103/PhysRevE.55.2203)

Mazloumian, A., Geroliminis, N. & Helbing, D. 2010 The spatial variability of vehicle densities as determinant of urban network capacity. *Phil. Trans. R. Soc. A* **368**, 4627–4647. (doi:10.1098/rsta.2010.0099)

Mueller, E. A. 1970 Aspects of history of traffic signals. *IEEE Trans.Veh. Technol.* **VT19**, 6–17. (doi:10.1109/T-VT.1970.23426)

MITSIM. Microscopic Traffic Simulator. See http://mit.edu/its/mitsimlab.html.

Nagatani, T. 2000 Traffic behaviour in mixture of different vehicles. *Physica A* **284**, 405–420. (doi:10.1016/S0378-4371(00)00263-6)

Nagel, K. & Schreckenberg, M. 1992 A cellular automaton model for freeway traffic. *J. Phys. I* **12**, 2221–2229. (doi:10.1051/jp1:1992277)

Nagel, K., Wagner, P. & Woesler, R. 2003 Still flowing: approaches to traffic flow and traffic jam modeling. *Oper. Res.* **51**, 681–710. (doi:10.1287/opre.51.5.681.16755)

Newell, G. F. 1961 Nonlinear effects in the dynamics of car following. *Oper. Res.* **9**, 209–229. (doi:10.1287/opre.9.2.209)

Newell, G. F. 2002 A simplified car-following theory: a lower order model. *Transport. Res. B* **36**, 195–205. (doi:10.1016/S0191-2615(00)00044-8)

NGSIM. Next Generation Simulation. See http://www.tfhrc.gov/about/ngsim.htm.

Orosz, G. & Stépán, G. 2006 Subcritical Hopf bifurcations in a car-following model with reaction-time delay. *Proc. R. Soc. A* **462**, 2643–2670. (doi:10.1098/rspa.2006.1660)

Orosz, G., Wilson, R. E., Szalai, R. & Stépán, G. 2009 Exciting traffic jams: nonlinear phenomena behind traffic jam formation on highways. *Phys. Rev. E* **80**, 046 205. (doi:10.1103/PhysRevE.80.046205)

Orosz, G., Moehlis, J. & Bullo, F. 2010 Robotic reactions: delay-induced patterns in autonomous vehicle systems. *Phys. Rev. E* **81**, 025 204(R). (doi:10.1103/PhysRevE.81.025204)

Payne, H. J. 1979 FREFLO: a macroscopic simulation model of freeway traffic. *Transport. Res. Rec.* **722**, 68–77.

Pipes, L. A. 1953 An operational analysis of traffic dynamics. *J. Appl. Phys.* **24**, 274–281. (doi:10.1063/1.1721265)

Powell, E. A. & Poehler, E. 2008 Rush hour in Pompeii: an archaeologist navigates first-century gridlock. *Archaeology* **61**, 18.

Prigogine, I. & Herman, R. 1971 *Kinetic theory of vehicular traffic.* Amsterdam, The Netherlands: Elsevier.

Roose, D. & Szalai, R. 2007 Continuation and bifurcation analysis of delay differential equations. In *Numerical continuation methods for dynamical systems* (eds B. Krauskopf, H. M. Osinga & J. Galan-Vioque), pp. 359–399. Understanding Complex Systems. Berlin, Germany: Springer.

Safonov, L. A., Tomer, E., Strygin, V. V., Ashkenazy, Y. & Havlin, S. 2002 Multifractal chaotic attractors in a system of delay-differential equations modeling road traffic. *Chaos* **12**, 1006–1014. (doi:10.1063/1.1507903)

Schönhof, M. & Helbing, D. 2009 Criticism of three-phase traffic theory. *Transport. Res. B* **43**, 784–797. (doi:10.1016/j.trb.2009.02.004)

Siebel, F. & Mauser, W. 2006 On the fundamental diagram of traffic flow. *SIAM J. Appl. Math.* **66**, 1150–1162. (doi:10.1137/050627113)

Sipahi, R. & Niculescu, S.-I. 2010 Stability of car following with human memory effects and automatic headway compensation. *Phil. Trans. R. Soc. A* **368**, 4563–4583. (doi:10.1098/rsta.2010.0127)

Swaroop, D., Hedrick, J. K., Chien, C. C. & Ioannou, P. A. 1994 A comparison of spacing and headway control laws for automatically controlled vehicles. *Veh. Syst. Dyn.* **23**, 597–625. (doi:10.1080/00423119408969077)

Treiber, M., Hennecke, A. & Helbing, D. 2000 Congested traffic states in empirical observations and microscopic simulations. *Phys. Rev. E* **62**, 1805–1824. (doi:10.1103/PhysRevE.62.1805)

Varaiya, P. 2008 Congestion, ramp metering and tolls. *Phil. Trans. R. Soc. A* **366**, 1921–1930. (doi:10.1098/rsta.2008.0015)

Wagner, P. 2010 Fluid-dynamical and microscopic description of traffic flow: a data-driven comparison. *Phil. Trans. R. Soc. A* **368**, 4481–4495. (doi:10.1098/rsta.2010.0122)

Ward, J. A. & Wilson, R. E. 2010 Criteria for convective versus absolute string instability in car-following models. Preprint.

Wilson, R. E. 2008 Mechanisms for spatio-temporal pattern formation in highway traffic models. *Phil. Trans. R. Soc. A* **366**, 2017–2032. (doi:10.1098/rsta.2008.0018)

Wilson, R. E., Berg, P., Hooper, S. & Lunt, G. 2004 Many-neighbour interaction and non-locality in traffic models. *Eur. Phys. J. B* **39**, 397–408. (doi:10.1140/epjb/e2004-00205-y)

Yeo, H. & Skabardonis, A. 2009 Understanding stop-and-go traffic in view of asymmetric traffic theory. In *Transportation and traffic theory 2009: Golden jubilee, 18th Int. Symp. of Traffic Theory and Transportation* (eds W. H. K. Lam, S. C. Wong & H. K. Lo), pp. 99–116. Berlin, Germany: Springer.

Zhang, J. & Ioannou, P. A. 2006 Longitudinal control of heavy trucks in mixed traffic: environmental and fuel economy considerations. *IEEE Trans. Intell. Transport. Syst.* **7**, 92–104. (doi:10.1109/TITS.2006.869597)

Zhou, J. & Peng, H. 2005 Range policy of adaptive cruise control vehicles for improved flow stability and string stability. *IEEE Trans. Intell. Transport. Syst.* **6**, 229–237. (doi:10.1109/TITS.2005.848359)